energies if the interactions are suddenly turned on.

[19]If initial correlations between particles are neglected, there is no advantage in expressing L_2(i.e., N) in terms of the $R^{(k)}$s [cf. Eq. (5.10)]; on the other hand, when initial correlations are included, it is hard to see the structure of L_2 if one does not make use of the $R^{(k)}$s.

[20]Note that the more general equation $M = N + \lambda M * N$ is obtained from (D1) by the transformation $M \to \lambda M$, $N \to \lambda N$, so that its solutions are obtained from those of (D1) by the same transformation.

[21]This is because if two successive collision times τ_i and τ_{i+1} in a product such as $\Pi_j m_{\Gamma_j}(\theta, \tau_j)$, $\theta < \tau_1 \leq \tau_2 \leq \tau_3 \ldots$, are separated by more than the maximum collision duration $t_{\max} \equiv \max\{t_{\Gamma_j}\}$, then the operators m_{Γ_j} separate into two time-disentangled groups, and the average $\langle\ \rangle$ of their product factorizes: $\langle \Pi_j m_{\Gamma_j} \rangle \to \langle \Pi_{j \leq i} m_{\Gamma_j} \rangle \langle \Pi_{j>i} m_{\Gamma_j} \rangle$. Now, the general term in $N_\theta(t, \tau)$ is of the form (5.6), with the correspondence $A_i(t, s_i) \to m_{\Gamma_i}(\theta, s_i)$ and $\Lambda \to P$; if for some i, $(s_{i+1} - s_i) > t_{\max}$, then the operator P appearing between m_{Γ_i} and $m_{\Gamma_{i+1}}$ has the same effect as the operator 1, which implies that the first two order terms in the density expansion of $N_\theta(t, \tau)$ exist in the limit $t \to -\infty$, by the same type of argument as those following Eq. (5.6).

[22]M. H. Ernst, L. K. Haines, and J. R. Dorfmann, Rev. Mod. Phys. 41, 296 (1969).

[23]J. Albers and I. Oppenheim, Physica 59, 161 (1972); 59, 187 (1972).

[24]R. Zwanzig, Phys. Rev. 129, 486 (1963).

[25]E. G. D. Cohen and R. Dorfman, Phys. Lett. 16, 124 (1965).

[26]S. Fujita, Phys. Lett. 22, 425 (1966); 24A, 235 (1967).

[27]B. C. Eu (report of work prior to publication).

[28]K. Kawasaki and I. Oppenheim, Phys. Rev. 129, A1763 (1965).

[29]Y. Pomeau, Phys. Rev. A 3, 1174 (1971).

PHYSICAL REVIEW A VOLUME 7, NUMBER 3 MARCH 1973

Simulation of Diatomic Homonuclear Liquids

J. Barojas*† and D. Levesque

Laboratoire de Physique Théorique et Hautes Energies, Faculté des Sciences, Bâtiment 211, 91-*Orsay, France*‡

B. Quentrec

Laboratoire de Chimie-Physique, Faculté des Sciences, 91-*Orsay, France*

(Received 21 August 1972)

The molecular-dynamic method was used to simulate a fluid of 500 rigid diatomic homonuclear molecules interacting by a double Lennard–Jones potential. The equilibrium and time-dependent properties are calculated in the liquid phase. The computed pressure and the internal energy agree quantitatively to a few percent with experimental values for nitrogen. The reorientational and the velocity of the center-of-gravity self-correlation functions are also discussed. The memory-function formalism and the extended-diffusion models are used to interpret the reorientational self-correlation functions. The analysis reveals that these self-correlation functions have an exponential behavior for times larger than 5×10^{-13} sec. In this model, considering present computing precision, there is no observable hydrodynamic-type relaxation in the reorientational self-correlation functions.

I. INTRODUCTION

The molecular-dynamic (MD) method has been widely used to study the monoatomic fluids.[1–3] Recent computer experiments, considering a Lennard–Jones (LJ) potential as the interaction between pairs of particles have lead to a determination of several thermodynamic properties (pressure, internal energy, and phase transition[4]), the equilibrium correlation functions,[5] the self-correlation function of the velocities, and the self-diffusion coefficients.[6] For argon, the calculated quantities agree within a few percent with the experimental data. The purpose of this comparison between computed and experimental values is not to demonstrate that the real potential is a LJ potential (for instance in argon), but to establish that the proposed model has all the significant physical properties of a real system. Then the simulated system can be considered as a reference for theoretical studies of equilibrium and transport properties.

Up to the present time very few MD results on polyatomic liquids have been obtained, mainly because the molecular interactions are badly known. To our knowledge, the only MD calculations on polyatomic fluids have been carried out by Harp and Berne[7] using a Stockmayer-type potential to simulate CO and N_2 and by Rahman and Stillinger[8] to simulate H_2O.

In this work, we study another type of interaction potential, the so-called diatomic potential.[9] This potential has been successfully used to determine

the structural properties and the phonon spectra for α solid nitrogen.[10,11] A two-dimensional MD calculation using the same potential[12] gave the expected qualitative behavior for the reorientational self-correlation functions (scf). We shall test the validity of the diatomic potential by taking liquid nitrogen as a reference. We have chosen this specific fluid, because the potential parameters are well determined and experimental data are available.

In Sec. II we describe in detail the simulated system and discuss the integration method used to solve the equations of motion. In Sec. III we give the computed pressure and internal energy for two isochores. These isochores are calculated at two nitrogen densities, at the triple point and near the boiling point. In Sec. IV, the scf are discussed and their relaxation times tabulated; the self-diffusion coefficients are also given. The analysis of the vectorial and tensorial scf reveal an exponential behavior at long times ($\sim 10^{-12}$ sec), but for the angular momentum scf, the decay is so fast that no prediction of their long-time behavior is possible. The velocity center of gravity scf are similar to those of monoatomic fluids, but show some particularities connected with the different types of relaxation of the velocity components parallel and perpendicular to the molecular axis. In Sec. V we consider two phenomenological approaches frequently used to interpret the reorientational scf; the memory-function formalism[3] and the extended diffusion models.[33] In the first approach, the introduction of the first few moments and the relaxation time is sufficient to describe satisfactorily the computed scf. But for the second one, despite the qualitative agreement between the computed and the approximated scf, no conclusion can be given about the validity of these models. Finally, in Sec. VI we discuss the connection between our results and previous computation on diatomic liquids.[7]

II. DESCRIPTION OF MODEL: INTEGRATION PROCEDURE

We consider a system of N rigid diatomic molecules contained in a cube of volume V with periodic boundary conditions. We take $N = 500$. The interaction between any two molecules j and k are characterized by the diatomic potential U_{jk} (Ref. 9, 10):

$$U_{jk} = \sum_{n=1}^{4} v(r_n) , \tag{1}$$

where

$$v(r) = 4\epsilon\,[(\sigma/r)^{12} - (\sigma/r)^{6}] ;$$

with the parameters[11] $\epsilon = 0.6067 \times 10^{-14}$ erg and $\sigma = 3.341$ Å. The r_n are the distances between the center of force associated with the nonbonded atoms of any two molecules. The centers of force are located at a distance d' from the molecular center of gravity, while the interatomic distance is $2d$, with $d = 0.1646\sigma$.[11]

We denote by $\vec{X}_j$ the position vector of the jth molecular center of gravity and by $\vec{u}_j$ a vector of magnitude d' going from the center of gravity to one atomic interaction center. Then the positions of the two atoms belonging to the jth molecule are

$$\vec{x}_j^{\,1} = \vec{X}_j + \alpha\,\vec{u}_j , \qquad \vec{x}_j^{\,2} = \vec{X}_j - \alpha\,\vec{u}_j , \tag{2}$$

where $\alpha = d/d'$. In most computations we put $\alpha = 1$. A schematic representation of the model is given in Fig. 1.

The kinetic energy of the system is written as

$$K = \tfrac{1}{2}m \sum_{j=1}^{N} [\dot{\vec{X}}_j^{\,2} + \alpha^2 \dot{\vec{u}}_j^{\,2}]$$

$$= \tfrac{1}{2}m \sum_{j=1}^{N} [\dot{\vec{X}}_j^{\,2} + d^2(\dot{\theta}_j^2 + \sin^2\theta_j\,\dot{\varphi}_j^2)] , \tag{3}$$

where m is the molecular mass. θ_j and φ_j are the angular coordinates of vector $\vec{u}_j$, as is shown in Fig. 2. We denote by $\vec{f}_{jk}$ the force between the centers of gravity of molecules j and k so that the equations of motion are

$$\ddot{\vec{X}}_j = \frac{1}{m} \sum_{k=1}^{N} \vec{f}_{jk} , \tag{4}$$

$$\ddot{\theta}_j = \sin\theta_j \cos\theta_j\,\dot{\varphi}_j^2 - \frac{1}{md^2} \sum_{k=1}^{N} \frac{\partial U_{jk}}{\partial \theta_j} , \tag{5}$$

$$\ddot{\varphi}_j = -2\cot\theta_j\,\dot{\theta}_j\,\dot{\varphi}_j - \frac{1}{md^2\sin^2\theta_j} \sum_{k=1}^{N} \frac{\partial U_{jk}}{\partial \varphi_j} . \tag{6}$$

These equations are of the form $\ddot{s}(t) = y(s(t), \dot{s}(t))$, where y is an arbitrary function. To solve them we use an algorithm[4] obtained by Taylor expansion of $s(t+\Delta t)$ and $s(t-\Delta t)$. By summing up both expansions we find

$$s(t+\Delta t) = 2s(t) - s(t-\Delta t) + (\Delta t)^2 y(s(t), \dot{s}(t)) + O(\Delta t^4) , \tag{7}$$

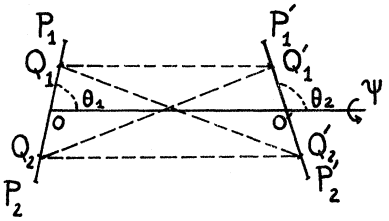

FIG. 1. Potential model used to simulate homonuclear diatomic liquids (Ref. 9). The four LJ interactions between neighboring molecules are indicated by dashed lines. For the first molecule, O represents the position of the center of gravity, P_1 and P_2 the atomic positions, and Q_1 and Q_2 the atomic interaction centers. The same with primes, for the second molecule. The molecular orientation angles are defined as follows: θ_1 and θ_2 are the polar angles measured relative to the vector connecting the centers of gravity of the interacting molecules, and ψ is the difference between their azimuthal angles.

and by subtracting them,

$$\dot{s}(t)=[s(t+\Delta t)-s(t-\Delta t)]/2\Delta t+O(\Delta t^3)\ . \quad (8)$$

This algorithm is useful only when the y function is independent of $\dot{s}(t)$, because Eq. (8) gives $\dot{s}(t)$ as a function of the unknown $s(t+\Delta t)$. Therefore, only the translational equation of motion can be solved by (7). To solve Eqs. (5) and (6), we compute $\dot{\theta}_j$ and $\dot{\varphi}_j$ by

$$\dot{\theta}_j(t+\Delta t)=\dot{\theta}_j(t)+\Delta t\,\dot{\theta}_j(t)+\tfrac{1}{2}\Delta t^2\,\dddot{\theta}_j(t)+O(\Delta t^3)$$
$$=\frac{1}{2\Delta t}\left[\tfrac{11}{3}\,\theta_j(t+\Delta t)-6\,\theta_j(t)+3\,\theta_j(t-\Delta t)\right.$$
$$\left.-\tfrac{2}{3}\,\theta_j(t-2\Delta t)\right]+O(\Delta t^3) \quad (9)$$

and

$$\sin^2\theta_j(t+\Delta t)\,\dot{\varphi}_j(t+\Delta t)=\sin^2\theta_j(t-\Delta t)\,\dot{\varphi}_j(t-\Delta t)$$
$$+2\Delta t\,\frac{\partial}{\partial t}\left[\sin^2\theta_j(t)\,\dot{\varphi}_j(t)\right]+O(\Delta t^3)\ . \quad (10)$$

Here, θ_j and φ_j are obtained from a relation similar to (7). The choice of these equations yield a good stability of the integration algorithm.

The term $\sin^2\theta_j$ in Eq. (6) introduces numerical errors in the computation of $\ddot{\varphi}_j$ when θ_j is nearly $0°$ or π. To avoid this difficulty, when $0°<\theta_j<\frac{1}{10}\pi$ or $\frac{9}{10}\pi<\theta_j<\pi$, we change the definition of the spherical angles θ_j, φ_j to θ'_j, φ'_j or vice versa.[8] This situation is shown in Fig. 2. As this change does not modify the expressions of the center-of-force Cartesian coordinates, the computations of the intermolecular forces are independent of the angular definitions. The previous algorithm, Eqs. (7)–(10), has been tested for a free rotator and for an N particle system in which density and temperature conditions are extreme. When we use it in a simulation of 800–1000 integration steps with $\Delta t=5\times10^{-15}$ sec, the relative variation for the total energy and the total linear momentum are of the order of $10^{-4}\sim10^{-5}$. Nonconservation of energy and total momentum is due to the LJ potential cutoff at $r_v=3.2\sigma$, to the algorithm which is only exact up to order $(\Delta t)^4$, and to the finiteness of the integration step.

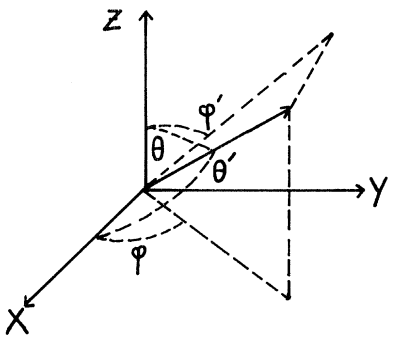

FIG. 2. Frames of reference used to measure the spherical angles θ and φ or θ' and φ', required to evaluate the components of the molecular orientation $\vec{u}(t)$.

The initial conditions for the integration process are selected in such a way that the positions of the molecular center of gravity and each molecular orientation correspond exactly to those of the nitrogen α phase.[10] Furthermore, translational and angular velocities are chosen according to a Maxwell distribution. Then the system evolves until equilibrium is reached. This condition is obtained, first, when the temperature and pressure do not systematically increase nor decrease, but both fluctuate about their average values, and second, when the density corresponds to a liquid phase, i.e., when the melting factor $\rho_k=\sum_{i=1}^{N}\cos(\vec{k}\cdot\vec{X}_i)$ varies between $+N^{1/2}$ and $-N^{1/2}$ (here $\vec{k}$ is the smallest vector of the reciprocal lattice). Once thermodynamic equilibrium is attained, we start the calculation of the average values and the evolution of the system is recorded.

Throughout our computation we use reduced units $r^*=r/\sigma$, $T^*=k_BT/\epsilon$, $\rho^*=\rho\sigma^3$, $P^*=(\sigma^3/\epsilon)P$, $t^*=t/\tau_0$, where T is the temperature, k_B the Boltzmann constant, ρ the molecular density, P the pressure, and t the time, with $\tau_0=(m\sigma/24\epsilon)^{1/2}=2.9848\times10^{-13}$ sec when the nitrogen molecular mass and the LJ parameters correspond to nitrogen.[11]

III. THERMODYNAMIC QUANTITIES AND STATIC PROPERTIES

In Sec. III A we give the computed internal energy and pressure and we define the radial pair-correlation functions in terms of which those thermodynamical quantities are expressed. In III B, we discuss these correlation functions. Finally, in III C we give the computed static structure factors. Comparison with experimental data for liquid nitrogen is given as well.

A. Thermodynamic Quantities

The internal energy is computed from

$$U_I=\frac{1}{N}\left\langle\sum_{j<k=1}^{N}U_{jk}\right\rangle \quad (11)$$

and the total pressure from the virial theorem

$$P=\rho k_BT+\frac{1}{3V}\left\langle\sum_{j<k=1}^{N}\vec{f}_{jk}\cdot\vec{X}_{jk}\right\rangle, \quad (12)$$

where ρ is the molecular density, $\vec{X}_{jk}=\vec{X}_j-\vec{X}_k$, and the brackets $\langle\cdots\rangle$ indicate time averages. The time-average quantities can be rewritten by introducing the atomic pair-distribution function

$$\rho(\vec{r}_1,\vec{r}_2,\Omega_1,\Omega_2)=(\rho^2/4\pi^2)g(\vec{r}_1,\vec{r}_2,\Omega_1,\Omega_2)\ . \quad (13)$$

This function represents the probability distribution of finding an atom of one molecule at $\vec{r}_1$, with

orientation Ω_1, and an atom of another molecule at $\vec{r}_2$, with orientation Ω_2. (Ω_j corresponds to the variables θ_j and φ_j characterizing the orientation of $\vec{u}_j$).

For liquids, the correlation function g depends only on $\vec{r}=\vec{r}_2-\vec{r}_1$ and on Ω, the relative orientation between Ω_1 and Ω_2. Then we can write

$$\int\int g(\vec{r}_1, \vec{r}_2, \Omega_1, \Omega_2)d\vec{r}_1 d\Omega_1 = 4\pi V g_0(\vec{r}, \Omega). \quad (14)$$

As the molecule has a cylindrical symmetry, $g_0(\vec{r}, \Omega)$ is only a function of r, θ, and Ω, when θ is the angle between $\vec{r}$ and the orientation vector $\vec{u}$ of one of the two molecules. We define

$$2\pi g_1(r, \theta)=\int g_0(r, \theta, \Omega)d\Omega\,,$$
$$g_2(r)=\int_0^{\pi} g_1(r, \theta)\sin\theta\, d\theta\,. \quad (15)$$

Then the internal energy given by (11) can be rewritten as

$$U_I = 16\pi\rho\int_0^{\infty} v(r)g_2(r)r^2 dr \quad (16)$$

and the pressure given by (12) as

$$P=\rho k_B T + P_1 + P_2\,, \quad (17)$$

where

$$P_1 = -\tfrac{2}{3}\pi\rho^2\int_0^{\infty}\frac{\partial v(r)}{\partial r}g_2(r)r^3 dr\,, \quad (18)$$

$$P_2 = -\tfrac{2}{3}\pi\rho^2 d'\int_0^{\infty}\frac{\partial v(r)}{\partial r}r^2 dr \times\int_0^{\pi} g_1(r, \theta)\cos\theta\sin\theta\, d\theta\,. \quad (19)$$

In the MD experiments we compute $g_2(r)$ for $r \leq 3.2\sigma$. The long tail corrections to Eqs. (16) and (18) are calculated by setting $g_2(r)=1$. In Eq. (19) we neglect this correction because in a fluid, for $r > r_v$ the correlation function $g_1(r, \theta)$ is almost independent of θ; hence, in (19) the angular integral vanishes. We have another kind of error in our values of P^* and U_I^* owing to the limited time averaging. These errors denoted by ΔP^* and by ΔU_I^* can be evaluated by comparison between several independent computations of the same duration and at the same ρ^* and T^*. The estimated values are $\Delta P^* \simeq 0.2-0.1$ and $\Delta U_I^* \simeq 0.1-0.05$.

The values for P^* and U_I^* are given in Table I. The comparison of the equation of state with experimental data for nitrogen[13] is done in Fig. 3. The densities of the two computed isochores are $\rho^* = 0.696$ and $\rho^* = 0.622$, and correspond, respectively, to triple-point and near-boiling-point densities. The agreement with experimental results is satisfactory and sufficient to establish the reliability of the model. The fact that at low temperature the P^* computed values are lower than the experimental ones and that at high temperature the situation is reversed could not be improved by rescaling the

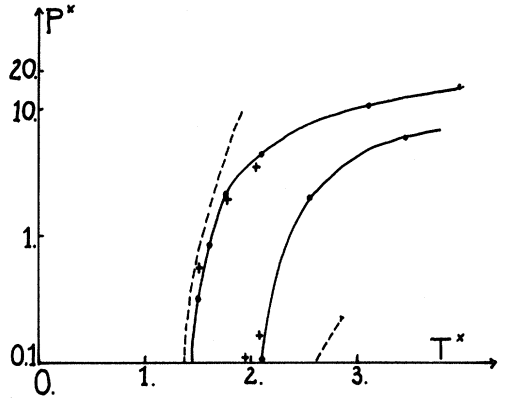

FIG. 3. Equation of state. Full lines give computed isochores; the upper one corresponds to $\rho^* = 0.696$ and the lower one to $\rho^* = 0.622$. Dots represent MD results and cross experimental values (Ref. 13) for liquid nitrogen. Dashed lines are the coexistence curves, between solid and liquid phases and between liquid and gas phases.

LJ parameters. We have modified the parameter $\alpha = d/d'$ without altering ϵ and σ. The results obtained at $\rho^* = 0.696$ and $T^* = 1.79$ are $P^* = 4.6$ for $\alpha = 0.9$, $P^* = 0.48$ for $\alpha = 1.1$, and $P^* = 2.1$ for $\alpha = 1$. The experimental pressure for nitrogen is $P^* = 2.0$. The value $\alpha = 1$ seems to correspond to the most realistic situation.

The equation of state can also be obtained from equilibrium perturbation theory.[14] The center-of-gravity radial correlation function $g_G(r)$ determined from this theory was compared with the MD results at triple point ($\rho^* = 0.696$ and $T^* = 1.5$).[15] The comparison between these functions gives an agreement similar to that reported by Sung and Chandler.[16] Nevertheless, the pressure computed from the theoretical $g_G(r)$ departs strongly from the MD data reported in this work.

B. Atomic Pair-Correlation Functions

We have defined in Eq. (15) the atomic pair-correlation functions $g_1(r, \theta)$ and $g_2(r)$. In Fig. 4, $g_2(r)$ is plotted at $\rho^* = 0.696$, $T^* = 1.83$ and 4.03. These functions differ strongly from the monoatomic pair-correlation function at the same thermodynamic state (for instance at triple point). The first peak of $g_2(r)$ is not so high, it is broader, and has two humps which correspond to the atoms of the nearest-neighbor molecule. Otherwise, the molecular center-of-gravity correlation function $g_G(r)$ looks like the monoatomic pair-correlation function at similar state, as it is shown in Fig. 4, where the $g_G(r)$ function is also given for the triple point ($\rho^* = 0.696$ and $T^* = 1.51$).

In order to determine the number of nearest molecules, we have computed the coordination number: $4\pi\rho\int_0^{r_m} g_2(r)r^2 dr$, where r_m corresponds to the first minimum of $g_2(r)$. For any temperature, the

TABLE I. Computed thermodynamical quantities. First and second columns give the density and the temperature of the system. Columns 3, 4, and 5 correspond, respectively, to pressures P^*, P_1^*, and P_2^*, evaluated from formulas (17), (18), and (19). Last column is the internal energy U_1^* given in (16). All these quantities are expressed in reduced units.

ρ^*	T^*	P^*	P_1^*	P_2^*	U_1^*
0.6220	2.12	0.026	−2.734	1.485	−16.35
	2.57	1.968	−1.293	1.667	−15.93
	3.48	5.812	+1.605	2.028	−15.10
0.6964	1.51	0.303	−2.636	2.099	−18.89
	1.62	0.824	−2.298	1.992	−18.75
	1.76	2.120	−1.246	2.152	−18.49
	2.12	4.208	+0.396	2.336	−18.06
	3.14	10.452	+5.375	2.918	−16.76
	4.03	15.239	+8.965	3.465	−15.77

value obtained at $\rho^* = 0.696$ is between 11 and 12, whereas from neutron diffraction experiments it is about 12[17] and from x-ray diffraction experiments[18] it is about 10.

The function $g_1(r, \theta)$ has been computed at $\rho^* = 0.696$ and $T^* = 1.53$ and is represented in Fig. 5, as a function of θ for several values of r. When r goes to infinity, $g_1(r, \theta)$ goes to 0.5. This value corresponds to an uncorrelated situation and it is attained approximately at $r = r_v$ (curve 5). But for smaller distances the curves show minima or maxima, implying the existence of strong correlations in the positions and in the orientation for the molecules in the three first-neighbor shells. Figure 6 gives an idea of the organization of the first-neighbor shell. There we sketched a rigid diatomic

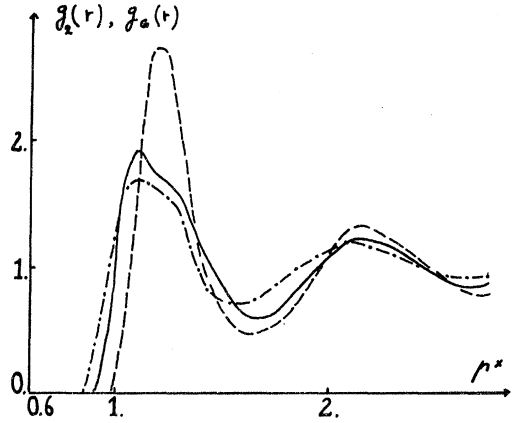

FIG. 4. Computed pair-correlation functions at triple-point density $\rho^* = 0.696$. Solid line represents the atomic pair-correlation function $g_2(r)$ at $T^* = 1.83$ and dot-dashed line the same function at $T^* = 4.03$. Dashed line corresponds to the molecular center-of-gravity pair-correlation function $g_G(r)$ at $T^* = 1.51$. The distance is in reduced units.

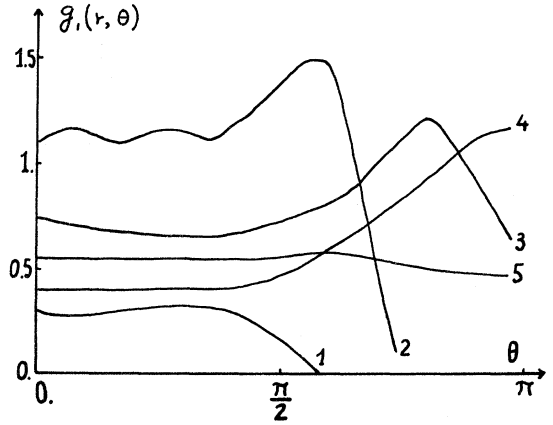

FIG. 5. Pair-correlation function $g_1(r, \theta)$ at $\rho^* = 0.696$ and $T^* = 1.53$. The distances in reduced units correspond respectively to: 0.94 (1); 1.10 (2); 1.30 (3); 1.39 (4); and 3.15 (5).

molecule by two circles of diameter $\frac{1}{2}\sigma$ whose centers are at a distance $2d$ (dumbbell molecule). As is expected, there is a symmetry with respect to an axis passing at the molecular center of gravity and perpendicular to the molecule axis. The most probable positions of the neighboring atoms are given by the maxima of $g_1(r, \theta)$. These maxima are situated on two circles of same radius and centered, respectively, on each atom of the reference molecule.

C. Static Structure Factor

Neutron- and x-ray-diffraction experiments in nitrogen[17,18] lead to the determination of the static structure factor $S(k)$. It is defined by

$$S(k) = \frac{1}{2N}\left\langle \left| \sum_{j=1}^{N} (e^{i\vec{k}\cdot\vec{x}_j^1} + e^{i\vec{k}\cdot\vec{x}_j^2}) \right|^2 \right\rangle$$

$$= \frac{2}{N}\left\langle \sum_{j\neq j'}^{N} e^{i\vec{k}\cdot(\vec{x}_j^1 - \vec{x}_{j'}^1)} \right\rangle$$

$$= \frac{1}{N}\left\langle \sum_{j=1}^{N} \cos 2\vec{k}\cdot\vec{u}_j \right\rangle + 1 . \qquad (20)$$

But, as the angular distribution of the vector $\vec{u}_j$ is uniform, we can write

$$S(k) = 1 + \sin(2kd)/2kd$$

$$+ 4\rho \int e^{i\vec{k}\cdot\vec{r}}[g_2(r) - 1]d^3r + 4\rho\delta(k) . \qquad (21)$$

This formula gives a very simple way to compute $S(k)$, if we know $g_2(r)$. But our MD calculations give $g_2(r)$ only for $r < r_v$, and we cannot use the approximation $g_2(r) = 1$ when $r > r_v$ because $S(k)$ will be poorly calculated for small k. Neither can we extrapolate $g_2(r)$ for long distance using Verlet's procedure, [5] because the interaction does not have spherical symmetry. Thus, the only way to compute $S(k)$ is by using Eq. (20) directly. In Fig. 7,

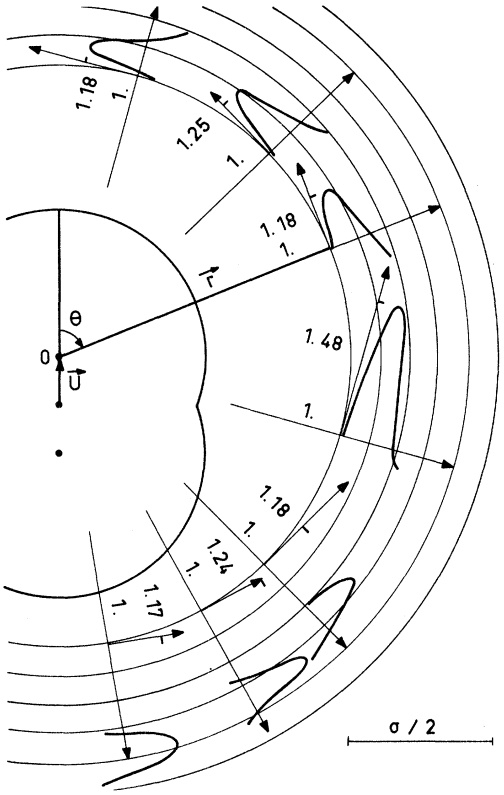

FIG. 6. Structure of the first-neighbor shell for a dumbbell molecule. The maximum of $g_1(r, \theta)$ is given for different orientations as a function of the distance, which is measured from the origin O in reduced units. The angle θ is measured from the $\vec{u}$ direction and dots represent the center of gravity and the atomic positions.

$S(k)$ is compared with the experimental results.[18] The first and second maxima of the computed $S(k)$ are located at $k = 0.942$ Å^{-1} and $k = 1.753$ Å^{-1} respectively. They correspond exactly with the experimental values, but their heights differ up to 8% for the first peak, 5% for the second one at triple-point density, and up to 7% and 6% for near-boiling-point density. In both cases the computed $S(k)$ seems to suggest a more regular arrangement of atoms than indicated by experimental results. Figure 8 shows the static structure factor at $\rho^* = 0.696$ for two different reduced temperatures, 1.83 and 4.03. The position of the first maximum is almost temperature independent at constant density, but its height decreases, indicating a progressive disappearance of the local order in the fluid, when the temperature is raised.

The errors in the calculation of $S(k)$, as well as in all computed quantities, are due to the limited number of time configurations. A second source of error in the calculation of $S(k)$ comes from the periodic boundary conditions which limit the number of $\vec{k}$ vectors with the same magnitude $|\vec{k}|$ entering in the evaluation of Eq. (20). Finally, the total error is estimated at 3–4%.

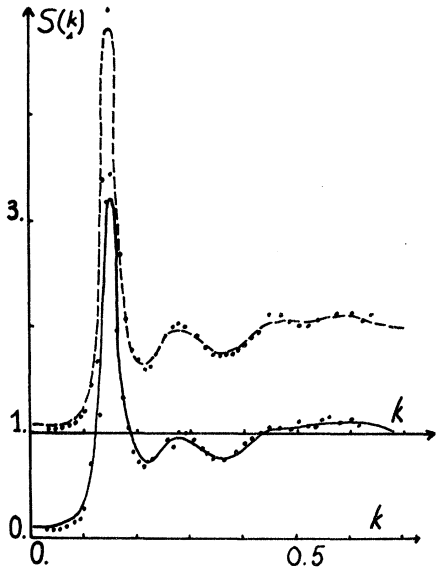

FIG. 7. Atomic static structure factor $S(k)$ for nitrogen. Experimental results (Ref. 18) are indicated by dashed line at the triple point ($\rho^* = 0.696$ and $T^* = 1.46$) and by solid line at the boiling point ($\rho^* = 0.649$ and $T^* = 1.75$). Dots represent the MD results at equivalent thermodynamical states. The k units are in Å$^{-1}/2\pi$.

IV. TIME-DEPENDENT SELF-CORRELATION FUNCTIONS

The scf of a microscopic quantity $A_i(t)$ associated to the ith molecule is computed in a MD experiment by the formula

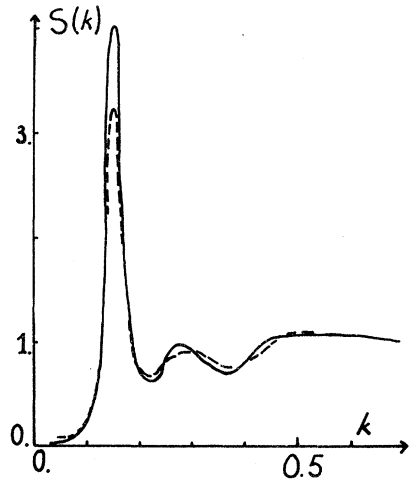

FIG. 8. Atomic structure factor at triple point density and two different temperatures. Solid line corresponds to $T^* = 1.83$ and dashed line to $T^* = 4.03$; k is measured in Å$^{-1}/2\pi$.

$$F_A(t) = \sum_{i=1}^{N} \int_0^T A_i(\tau) A_i(t+\tau)\, d\tau \Big/ \sum_{i=1}^{N} \int_0^T A_i(\tau) A_i(\tau)\, d\tau$$
$$= \langle A(0)A(t)\rangle / \langle A^2(0)\rangle \,, \qquad (22)$$

where T is the duration of the simulation ($T \simeq 10^{-11}$ sec).

In this section we study the scf associated with $\vec{u}_i(t)$, $\dot{\vec{X}}_i(t)$, and $J_i(t) = m\vec{u}_i(t) \times \dot{\vec{u}}_i(t)$, the angular momentum about the center of gravity of the molecule. We denote these functions by $F_V(t)$, $F_G(t)$, and $F_J(t)$, respectively. We also study the function $F_T(t)$:

$$F_T(t) = \tfrac{1}{2}\left[3\langle(\vec{w}(0)\cdot\vec{w}(t))^2\rangle - 1\right], \qquad (23)$$

where $\vec{w}_i(t) = \vec{u}_i(t)/d'$. The functions $F_V(t)$ and $F_T(t)$ are known as the first and second spherical harmonics of the molecular orientation. The properties of these five functions have been discussed extensively elsewhere.[19]

In the reported MD experiments, the maximum value of t is $6.7\,\tau_0 = 2.0\times10^{-12}$ sec, but for times greater than $4\tau_0 \simeq 1.2\ 10^{-12}$ sec the statistical fluctuations have the same order of magnitude as the value of the scf (about 0.02).

A. Reorientational scf

For a free rotator the reorientational scf are given by

$$F_V^0(t) = \int_0^\infty \omega e^{-\omega^2/2}\cos(\omega t)\, d\omega \,, \qquad (24)$$

$$F_T^0(t) = \tfrac{1}{4}\int_0^\infty \omega e^{-\omega^2/2}\left[3\cos(2\omega t) + 1\right] d\omega \,. \qquad (25)$$

Comparison with the computed scf (Figs. 9 and 10) leads to the conclusion that the rotational motion in the simulated liquid is strongly hindered.

For short times, $t < 6.0\times10^{-13}$ sec, $F_V(t)$ and $F_T(t)$ decay more rapidly for increasing temperature and decreasing densities as expected by time expansion.[20] But, for $t > 6.0\times10^{-13}$ sec the situation is not the same. When $\rho^* = 0.696$ and $T^* \leq 2.3$, and $\rho^* = 0.622$ and $T^* \leq 2.6$, both scf decay exponentially. The characteristic time of the exponentials are nearly equal and are not very sensitive to temperature and density variations. At higher temperature than those mentioned before, these scf decay so rapidly than the statistical errors prevent any accurate analysis for large time. This behavior is shown in Fig. 11 in semilogarithmic scale. There we also compare $F_T(t)$ at the boiling point ($T^* = 1.75$, $\rho^* = 0.640$) with the same scf given by Gordon[20] from Raman depolarized diffusion data.[21] The agreement is only qualitative for $t > 0.3\times10^{-12}$ sec.

The angular momentum scf $F_J(t)$ are nearly independent of temperature and decay faster at higher densities. As shown in Fig. 12, these functions decrease rapidly towards zero and have no negative region, implying that $\vec{J}$ is quickly decorrelated by "collisions" between molecules. These results are partially explained for short times by a weak dependence of the second moment of $F_J(t)$ on T^*. For long times and at $\rho^* = 0.622$ and $T^* = 2.12$, $F_J(t)$ decays exponentially; but for $\rho^* = 0.696$, the decay is too fast to obtain information on the long-time behavior owing to the statistical error.

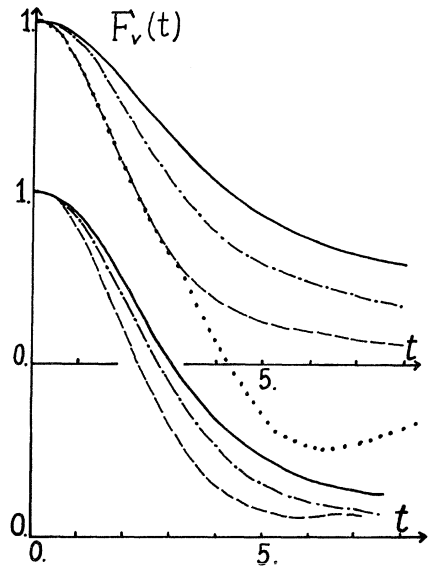

FIG. 9. Computed vectorial scf $F_V(t)$. Upper curves correspond to triple-point density $\rho^* = 0.696$, where the solid line is at $T^* = 1.43$, the dot-dashed line at $T^* = 2.30$, and the dashed line at $T^* = 4.03$. Lower curves give results near boiling-point density $\rho^* = 0.622$, where the solid line is at $T^* = 2.12$, the dot-dashed line at $T^* = 2.57$, and the dashed line at $T^* = 3.48$. Each division in time axis corresponds to 10^{-13} sec. Dotted line represents the free-rotator scf $F_V^0(t)$ at $T^* = 4.03$.

The relaxation times τ_A defined by

$$\tau_A = \int_0^\infty F_A(t)\, dt \qquad (26)$$

are given in Table II. It must be noted that τ_A is very different from the characteristic time of the exponential tail of $F_A(t)$ because, when it occurs, the tail starts at times $t > 0.5\times10^{-12}$ sec.

From NMR experiments on nitrogen the relaxation time τ_T has been determined at temperatures between 63 and 91 °K under equilibrium vapor pressure.[22] At the boiling point the value is 2.2×10^{-13} sec, while the MD result is $\tau_T = 2.4\times10^{-13}$ sec; the agreement is good considering that the uncertainty of the experimental value is of the order of 10%. For this relaxation time τ_T the authors[22] report an Arrhenius behavior: $\tau_T = ce^{-E/k_BT}$, with an activation energy E estimated in 100 ± 30 kcal/mole. Along the triple-point isochore and in the same range of temperatures ($1.4 \leq T^* \leq 2.3$) the MD results can also be approximated by an Arrhenius behavior with $E = 118$ kcal/mole. Nevertheless, the

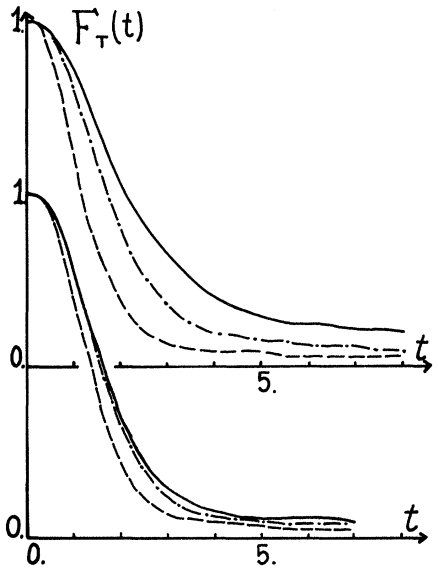

FIG. 10. Same as Fig. 9 for the computed tensorial scf $F_T(t)$.

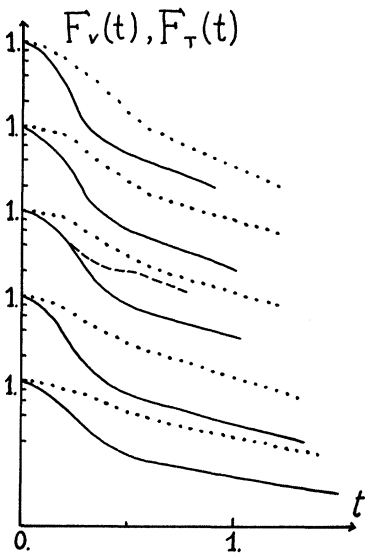

FIG. 11. Reorientational scf in a semilogarithmic scale. Solid lines represent $F_T(t)$ and dotted lines $F_V(t)$. In central curves the dashed line corresponds to Gordon's result.[20] From top to bottom, these curves are obtained at: $\rho^* = 0.622$ and $T^* = 2.58$; $\rho^* = 0.622$ and $T^* = 2.10$; $\rho^* = 0.640$ and $T^* = 1.75$; $\rho^* = 0.696$ and $T^* = 2.30$; and $\rho^* = 0.696$ and $T^* = 1.43$ (triple point). Time is given in units of 10^{-12} sec.

E value is so small that in this range of temperature, τ_T would be as well represented by a linear function of T^{*-1}.

B. Molecular Center of Gravity Velocity scf

The scf $F_G(t)$ are given in Fig. 13. As in monoatomic liquids,[2] they have a negative plateau. At $\rho^* = 0.622$ this negative region is only present at low temperatures. However, at $\rho^* = 0.696$, $T^* = 1.43$ and 1.83 there exist two minima near $t = 3 \times 10^{-13}$ and 6×10^{-13} sec, which disappear at higher T^*. This fact is associated with two very different behaviors of the scf at small times. One relaxation behavior is related with the $\vec{\dot{X}}(t)$ component parallel to $\vec{u}(0)$ and the other one to the perpendicular component. We define

$$F_G^{\parallel}(t) = \langle \vec{\dot{X}}^2 \rangle^{-1} \langle [\vec{w}(0) \cdot \vec{\dot{X}}(0)] [\vec{w}(0) \cdot \vec{\dot{X}}(t)] \rangle , \quad (27)$$

$$F_G^{\perp}(t) = \langle \vec{\dot{X}}^2 \rangle^{-1} \langle [\vec{s}(0) \cdot \vec{\dot{X}}(0)] [\vec{s}(0) \cdot \vec{\dot{X}}(t)] \rangle , \quad (28)$$

where $\vec{s}$ is a unit vector perpendicular to $\vec{u}$.

Then we have

$$F_G(t) = F_G^{\parallel}(t) + 2F_G^{\perp}(t) . \quad (29)$$

The computation of $F_G^{\parallel}(t)$ and $F_G^{\perp}(t)$ has been done at $\rho^* = 0.696$, $T^* = 1.83$ and 4.03. The results are plotted in Fig. 14. They confirm the precedent interpretation of the two minima in $F_G(t)$.

The self-diffusion coefficient D is given by $D = k_B T \tau_G / m$. The MD values are given in Table II and can only be compared with an estimation given by Sears,[23] using the law of corresponding states between argon and nitrogen. He gives $D = 3.7 \times 10^{-5}$ $cm^2 sec^{-1}$ at boiling point and we find $D = 2.5 \times 10^{-5}$ $cm^2 sec^{-1}$.

V. MODEL INTERPRETATION FOR REORIENTATIONAL SELF-CORRELATION FUNCTIONS

The most important aspect of the self-motion in liquids can be described by two phenomenological

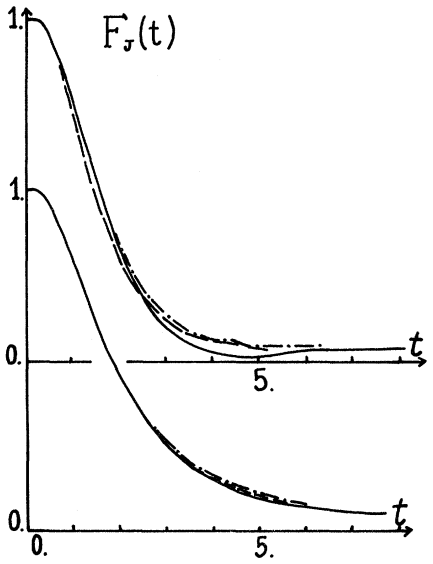

FIG. 12. Same as Fig. 9 for the computed angular momentum scf $F_J(t)$.

TABLE II. Computed relaxation times and self-diffusion coefficients. First and second columns give, in reduced units, the density and the temperature of the system. The next four columns correspond to computed relaxation times in 10^{-12} sec. Last column indicates the self-diffusion coefficient in 10^{-5} cm^2 sec^{-1}.

ρ^*	T^*	τ_V	τ_T	τ_J	τ_G	D
	2.12	0.41	0.22	0.24	0.13	3.59
0.6220	2.57	0.32	0.19	0.24	0.13	4.36
	3.48	0.27	0.16	0.24	0.13	5.90
0.6400	1.75	0.47	0.24	0.24	0.11	2.52
	1.43	0.71	0.34	0.17	0.04	0.75
0.6964	1.83	0.55	0.28	0.17	0.06	1.43
	2.30	0.46	0.24	0.17	...	...
	4.03	0.28	0.15	0.17	0.08	4.21

approaches: the memory-function formalism and the stochastic models. In Sec. V A the memory-function formalism is summarized and an application to the reorientational MD results is given. In Sec. V B one of the stochastic models, the extended-diffusion model, is compared to exact scf. In both approaches, the parameters defining the models are taken from the MD experiments.

A. Memory-Function Formalism

The time evolution of the scf $F_A(t)$, defined in (22), is given by[24,25]

$$\frac{\partial F_A(t)}{\partial t} + \int_0^t M_A^0(t-t')F_A(t')\,dt' = 0, \tag{30}$$

where the kernel $M_A^0(t)$ has the meaning of a memory or retarded-effect function and can be considered as a generalized friction coefficient nonlocal in time. This kernel also satisfies an equation similar to (30), in which a new memory function $M_A^1(t)$ is introduced. In this way, an infinite set of memory functions is obtained; these functions are related to each other by a hierarchy of coupled equations. Consider the Fourier-Laplace transform definitions

$$\tilde{F}_A(\omega) = \int_0^\infty e^{i\omega t} F_A(t)\,dt \tag{31}$$

and

$$\tilde{M}_A^i(\omega) = \int_0^\infty e^{i\omega t} M_A^i(t)\,dt\,, \tag{32}$$

where $i = 0, 1, 2, \ldots$. Then Eq. (30) can be written as

$$\tilde{F}_A(\omega) = F_A(0)/\left[-i\omega + \tilde{M}_A^0(\omega)\right] \tag{33}$$

and the hierarchy as

$$\tilde{F}_A(\omega) = \cfrac{F_A(0)}{-i\omega + \cfrac{M_A^0(0)}{-i\omega + \cfrac{M_A^1(0)}{-i\omega + \ldots}}} \tag{34}$$

The values of the $M_A^i(0)$ are defined in terms of successive derivatives of $F_A(t)$ at $t = 0$.

In order to use (34), a decoupling procedure must be given by assuming at some stage a simple analytical form for $M_A^i(t)$; usually an exponential or Gaussian form is chosen:

$$M_A^0(t) = M_A^0(0)\,e^{-\alpha_A t}$$

or

$$M_A^0(t) = M_A^0(0)\,e^{-(\pi/4)\alpha_A^2 t^2}\,, \tag{35}$$

$$M_A^1(t) = M_A^1(0)\,e^{-\gamma_A t}$$

or

$$M_A^1(t) = M_A^1(0)\,e^{-(\pi/4)\gamma_A^2 t^2}\,. \tag{36}$$

When one of these forms has been chosen, we may either consider $M_A^0(0)$, $M_A^1(0)$, α_A, and γ_A as parameters or determine them in such a way that certain known data on the scf is reproduced. In general, $M_A^0(0)$ and $M_A^1(0)$ are chosen to give the greatest number of exact $F_A(t)$ derivatives at $t = 0$, being defined in terms of the mean-square values of dynamical quantities and the molecular moment of inertia.[3] The $M_A^0(0)$ and $M_A^1(0)$ values which are not simple functions of the temperature are given

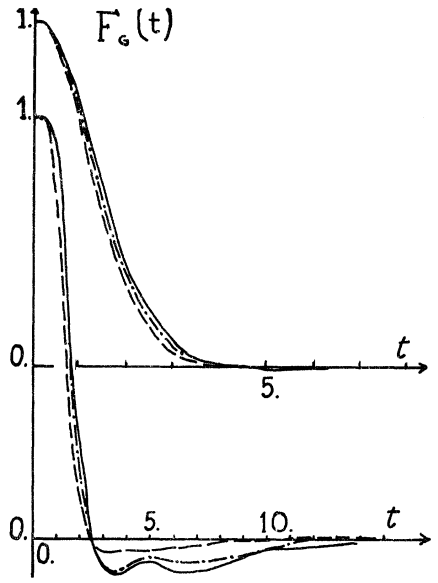

FIG. 13. Computed center-of-gravity velocity scf $F_G(t)$. Upper curves represent near-boiling-point results at $\rho^* = 0.622$, where the solid line is at $T^* = 2.12$, the dot-dashed line at $T^* = 2.57$, and the dashed line at $T^* = 3.48$. Lower curves give the triple-point results at $\rho^* = 0.696$, where the solid line is at $T^* = 1.43$, the dot-dashed line at $T^* = 1.83$, and the dashed line at $T^* = 4.03$. In both curves the time unit is 10^{-13} sec.

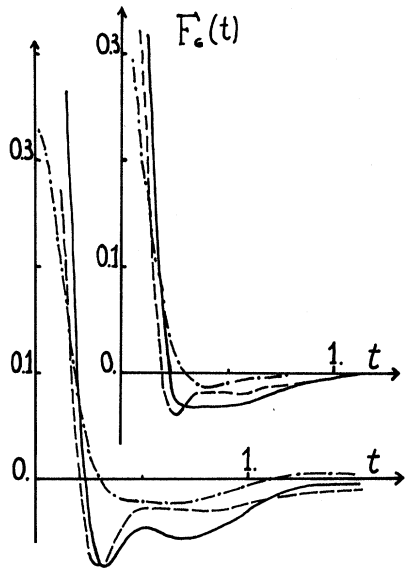

FIG. 14. Analysis of the relaxation behavior in $F_G(t)$ at triple-point density $\rho^* = 0.696$. Upper curves correspond to $T^* = 4.03$ and lower ones to $T^* = 1.83$. In both cases, the solid lines represent $F_G(t)$, the dot-dashed lines $F_G^{\parallel}(t)$, and the dashed lines $2F_G^{\perp}(t)$. Time scale is in 10^{-12} sec.

in Table III. The two other quantities, α_A and γ_A, are chosen to obtain equal relaxation times of the scf calculated from (35) and (36) and from MD computation. With this choice the approximations (35) correspond to two and three exact $F_A(t)$ derivatives at $t = 0$. Then, from (33) we obtain

$$\alpha_A = \tau_A M_A^0(0) . \tag{37}$$

The approximations (36) correspond to four and five exact $F_A(t)$ derivatives at $t = 0$. Thus, from (34),

$$\gamma_A = M_A^1(0)/M_A^0(0)\,\tau_A . \tag{38}$$

The exponential memory functions give a very simple analytical representation of the scf just by linear combination of exponentials. This result comes from the fact that the denominator in Eq. (34) is a polynomial in ω. On the other hand, an advantage of the Gaussian memory functions is to present the correct time-parity in the scf. However, at the same order of approximation in the hierarchy (34), both analytical forms lead to similar results.

We show in Fig. 15 an example of the application of the approximation given by Eq. (35). Comparison between the scf derived from this approximation and the vectorial scf $F_V(t)$ at $\rho^* = 0.696$ and $T^* = 1.83$ gives a very poor result. In the exponential case the disagreement is stronger than in the Gaussian case, because the former short-time behavior is not correct. Moreover, the exponential decay observed in Fig. 11 is not well reproduced. The next order approximation in the memory function, Eq. (36), is given in Fig. 16 for the same scf at the same thermodynamical state. Here the agreement between postulated and exact scf is satisfactory, being good at short times, and for $t > 10^{-12}$ sec both functions differ in quantities of the background-noise order (estimated in ± 0.02). Also, in this approximation the long-time exponential decay is well reproduced. In fact, from the MD results the decaying characteristic time of this

TABLE III. Mean-square values for the center-of-gravity acceleration $\langle a^2 \rangle$ and the torque about the molecular center of gravity $\langle R^2 \rangle$. First and second columns give, in reduced units, the density and the temperature of the system. In the third column $\langle a^2 \rangle$ is given in 10^{36} $(\mathrm{cm/sec^2})^2$ and in fourth column $\langle R^2 \rangle$ in 10^{-28} ergs^2. The corresponding conversion factors to reduced units are $\langle a^2 \rangle = 14.0595 \times 10^{34} \langle a^{*2} \rangle$ and $\langle R^2 \rangle = 8.4807 \times 10^{-26} \langle R^{*2} \rangle$.

ρ^*	T^*	$\langle a^2 \rangle$	$\langle R^2 \rangle$
	2.12	6.69	21.29
0.6220	2.57	8.97	27.74
	3.48	14.27	44.12
0.6400	1.75	5.33	16.79
	1.43	5.10	16.45
0.6964	1.83	7.55	23.40
	3.14	17.02	52.41
	4.03	24.56	75.98

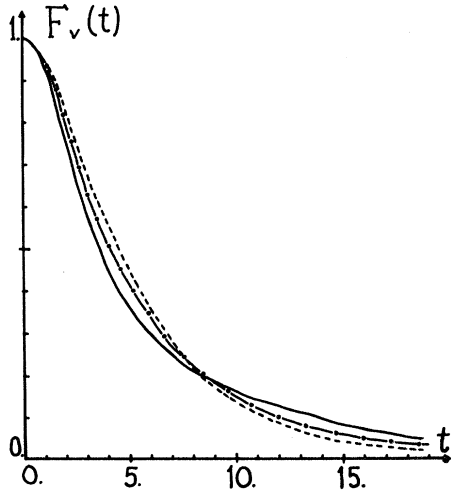

FIG. 15. Comparison between the memory-function formalism and the MD results for the vectorial scf $F_V(t)$ at $\rho^* = 0.696$ and $T^* = 1.83$. The exact scf is in solid line and the scf derived from postulated memory functions [Eq. (35)] are indicated by a dashed line for the exponential case and by a dot-dashed line for the Gaussian case. Time scale is in 10^{-13} sec.

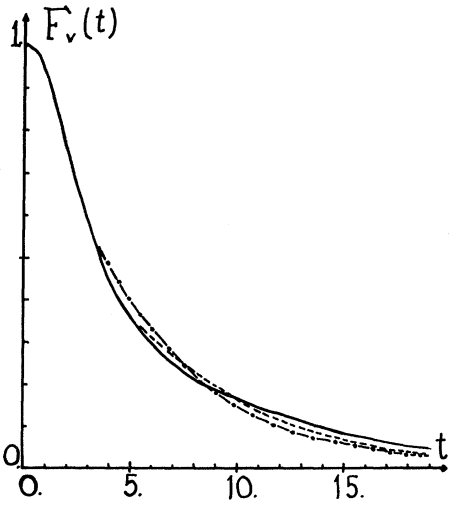

FIG. 16. Same as Fig. 15 for a higher-order approximation in the memory functions [Eq. (36)].

scf is equal to $2.0\tau_0$, while from the exponential memory function given in (36), it is equal to $1.9\tau_0$. For all thermodynamical states reported here, the denominator in (34) has always two complex roots and one real root. The later corresponds to the longest decay time. It is this time which reproduces correctly the behavior shown in Fig. 11. For instance, the values obtained from the MD and from the analytical solution of Eq. (34) are, respectively, $2.4\tau_0$ and $2.5\tau_0$ at $\rho^* = 0.696$ and $T^* = 1.43$, and $1.0\tau_0$ and $1.1\tau_0$ at $\rho^* = 0.696$ and $T^* = 4.03$.

In conclusion, the previous study shows that the knowledge of the first two moments and the relaxation time are enough to represent $F_V(t)$. This representation is limited by the errors produced in the MD calculation, their estimation summing up for 3–4% with a noise background of the order of ± 0.02 for $t > 10^{-12}$ sec. Therefore, taking into account that the model simulated here seems quite realistic, any experimental study of $F_V(t)$ which lacks a higher precision than the MD results will probably give very little information about the details of molecular motion in diatomic liquids. In fact, from a knowledge of $F_V(t)$ with an MD precision we can only deduce the values of the relaxation time τ_V and the mean-square torque $\langle R^2 \rangle$.

The MD angular momentum scf $F_J(t)$ at $\rho^* = 0.696$ and $T^* = 1.83$ is compared to Fig. 17 with the scf obtained from approximations (35). At intermediate times ($t \simeq 5 \times 10^{-13}$ sec) the agreement between the exact and the postulated scf is somewhat better than for $F_V(t)$ at the same order of approximation. For $t > 10^{-12}$ sec, the agreement is also satisfactory owing to the rapid decorrelation observed in $F_J(t)$. In order to improve the agreement, it would be necessary to introduce the next moment, which requires the computation of the mean-square value of the time derivative of the torque $\langle \dot{R}^2 \rangle$.

The memory-function formalism cannot be applied to analyze the tensorial scf $F_T(t)$, and for $F_G(t)$ it is more complicated. However, the formalism is well adapted to describe $F_V(t)$ and $F_J(t)$, in particular because their structure is very simple—they are always positive and decay exponentially or go to zero very rapidly (Figs. 9 and 12). At times $t \simeq 10^{-12}$ sec these two scf do not have the complex structure of $F_G(t)$; in particular, the structure of $F_J(t)$ gives no indication about the existence of an hydrodynamical behavior. [26,27]

B. Stochastic Models

The reorientational motion in liquids has been discussed as a binary collision process. Generally, this process is governed by a Poisson distribution

$$P(n, t) = \frac{1}{n!}\left(\frac{t}{\tau}\right)^n e^{-t/\tau}, \tag{39}$$

which gives the probability for one molecule to bring about n collisions during a time t, τ being the mean time interval between two collisions.

The models differ in the description of the collision effect on the angular momentum $\vec{J}(t)$. [28–34] It is assumed that the collision randomizes at least the orientation of $\vec{J}$ and that each collision terminates a free rotation step characterized by its angular frequency ω_n.

Following Gordon, [33] the vectorial scf $F_V(t)$ can be written as

$$F_V(t) = \sum_{n=0}^{\infty}\left(\frac{n!}{\tau^n}\right)\left[\int_0^t dt_n \cos\omega_{n+1}(t - t_n)\right.$$

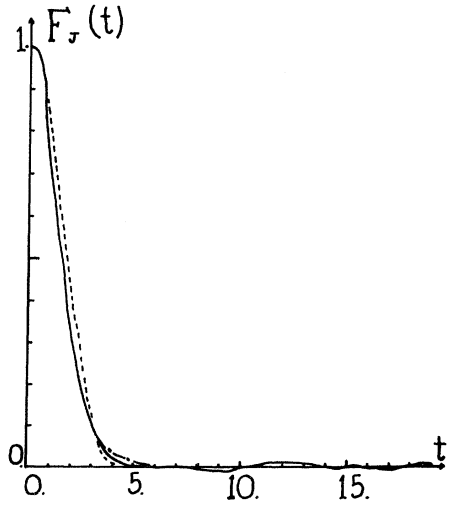

FIG. 17. Same as Fig. 15 for the angular momentum scf $F_J(t)$.

$$\times\int_0^{t_n} dt_{n-1}\cos\omega_n(t_n-t_{n-1})$$

$$\cdots\int_0^{t_2} dt_1\cos\omega_2(t_2-t_1)\cos\omega_1 t_1\Big] P(n,\,t)\ . \tag{40}$$

A similar procedure can be applied to compute the tensorial scf when $\cos\omega_n t$ is replaced by $\frac{1}{4}[3\times\cos(2\omega_n t)+1]$. The effect of the collision is then considered in two extreme situations, the so-called M diffusion and J diffusion. The reorientational scf will be denoted by two indexes, one index X describing the type of model M or J and another index l specifying the order of the spherical harmonics. Then from (40) and (39)

$$F_X^l(t)=e^{-t/\tau}G_X^l(t)\ , \tag{41}$$

with

$$G_X^l(t)=\sum_{n=0}^{\infty}\frac{1}{\tau^n}\int_0^t dt_n f_X^l(t-t_n)\int_0^{t_n} dt_{n-1} f_X^l(t_n-t_{n-1})$$

$$\cdots\int_0^{t_2} dt_1 f_X^l(t_2-t_1)f_X^l(t_1)\ , \tag{42}$$

where the functions $f_X^l(t)$ will be explicited later on.

In the M-diffusion model only the orientation of $\vec{J}$ is randomized by the collision, and all the angular velocities ω_n are equal to ω. This frequency is distributed over a classical Maxwell distribution and

$$F_M^l(t)=e^{-t/\tau}\int_0^{\infty}\omega e^{-\omega^2/2}G_M^l(t)\,d\omega\ . \tag{43}$$

Here $G_M^l(t)$ is given in (42) and

$$f_M^1(t)=\cos(\omega t)\ , \tag{44}$$

$$f_M^2(t)=\tfrac{1}{4}[3\cos(2\omega t)+1]\ . \tag{45}$$

In the J-diffusion model, both magnitude and direction of $\vec{J}$ are randomized by the collision, and the angular velocity at one step is statistically independent of the angular velocity at the step before. For each collision step the randomization of the magnitude of $\vec{J}$ is introduced by an average over a Maxwell distribution. Then

$$F_J^l(t)=e^{-t/\tau}G_J^l(t)\ , \tag{46}$$

with $G_J^l(t)$ given in (42) and, using Eqs. (24) and (25),

$$f_J^l(t)=\int_0^{\infty}\omega e^{-\omega^2/2}f_M^l(t)\,d\omega=\begin{cases}F_V^0, & l=1\\ F_T^0, & l=2\end{cases}\ . \tag{47}$$

Formula (42) has been computed using matrix-multiplication method[33,34]; however, it is completely equivalent to next integral equation

$$G_X^l(t)=f_X^l(t)+(1/\tau)\int_0^t f_X^l(t-s)\,G_X^l(s)\,ds\ , \tag{48}$$

which can be solved numerical or in terms of Laplace transforms, when the functions $f_X^l(t)$ are simple.[3,31] Then, for the M model we obtain

$$G_M^1(t)=e^{t/2\tau}\begin{cases}\cosh[t(1-\beta)^{1/2}/2\tau] + (1-\beta)^{-1/2}\sinh[t(1-\beta)^{1/2}/2\tau], & \beta<1\\ 1+t/2\tau\ , & \beta=1\\ \cos[t(\beta-1)^{1/2}/2\tau] + (\beta-1)^{-1/2}\sin[t(\beta-1)^{1/2}/2\tau], & \beta>1\end{cases}\ , \tag{49}$$

with $\beta=4\omega^2\tau^2$, and

$$G_M^2(t)=e^{t/3\tau}\begin{cases}A\,e^{2at}+e^{-at}[B_1\cos(bt)-B_2\sin(bt)], & \beta\neq\frac{8}{9}\\ A\,e^{2at}+C\,e^{-at}\ , & \beta=\frac{8}{9}\end{cases} \tag{50}$$

where the quantities A, B_1, B_2, a, and b are all determined in terms of the poles of Eq. (48). Using (49), (50), and (41), the vectorial and the tensorial scf will be obtained for the M model. For the J model, Eq. (48) must be integrated numerically. In all cases the simulated scf are between the corresponding M- and J-model predictions. With the computed values for $\tau=\tau_J$, the comparison with exact scf is satisfactory up to 10% at low densities and at higher temperatures.

Starting from rather different hypothesis, the phenomenological approaches previously discussed in Secs. V A and V B lead to a similar conclusion: At long times the exponential behavior is dominant, and this fact agrees with MD results. However, the hypothesis of the stochastic models leads to rather complicated analytical expressions and the flexibility of these models to reproduce the MD results is reduced, owing to the fact that only one parameter can be adjusted to give the adequate relaxation. Otherwise, the fourth moment is not included; this explains the difference between approximate and exact scf at intermediate times. Though the description of the scf can be improved, even for condensed systems, the stochastic models oversimplify the interpretation of the reorientational process. In fact, in some situations the agreement between the MD results and the stochastic models, represented by the extended-diffusion models, is semiquantitatively correct. However, the agree-

ment between a theoretical prediction and an experimental result, coming from a simulation or from a physical experiment, is not an absolute guarantee of the validity of the hypothesis in which such predictions are supported.

Indeed, as we have seen, the memory-function formalism gives a quite good description of the reorientational scf with only three parameters. Thus, any other representation of the reorientational scf will contain, at most, the dynamical information given essentially by the torque and the relaxation time. Therefore, the validity of the stochastic models is relative and their utility limited, because their simplicity masks the real dynamical behavior and in the best situation the provided information is restricted. In order to test the general hypothesis of the stochastic models we have applied the MD method to follow the motion of any one of the molecules of the system and then computed the quantity $\vec{u}(0)\cdot\vec{u}(t)$, during a time equivalent to 10^{-11} sec. We observe that the molecule spends a time of the order of 3×10^{-13} sec in a given orientation and then jumps into a new orientation in a time of the same order of magnitude. This shows that at least angular displacements are not small and that collisions have a finite time duration. A similar calculation on $\vec{J}(0)\cdot\vec{J}(t)$ shows that this quantity fluctuates randomly and that, reasonably, there is no time interval during which the molecule behaves as a free rotator. This behavior was confirmed by several runs at triple point by following different molecules.

VI. CONCLUSIONS

The previously reported results show that the equilibrium properties of the simulated model have all the characteristics of a fluid of diatomic homonuclear molecules. In fact, when the parameters ϵ, σ, and α are well chosen, the equation of state and the structure factor $S(k)$ agree nearly quantitatively with nitrogen experimental values. With respect to the reorientational scf $F_V(t)$ and $F_J(t)$, the first one represents a qualitative behavior similar to the same scf computed by Harp and Berne with a modified Stockmayer potential. However, the present model gives a rather different structure for $F_J(t)$ because the angular moment is decorrelated by the "collisions" between the repulsive core of the LJ potentials and not by the effect of dipolar or quadrupole couplings as in the modified Stockmayer potential. [35,36]

ACKNOWLEDGMENTS

We are indebted to Professor L. Verlet and Professor C. Brot for many suggestions and discussions during the realization of this work. We acknowledge their interest and encouragements.

*Permanent address: Facultad de Ciencias, U.N.A.M., México 20, D.F. México.

†Work supported by Consejo Nacional de Ciencia y Tecnología, México.

‡Laboratoire associé au Centre National de la Recherche Scientifique, Orsay, France.

[1]B. J. Alder and T. E. Wainwright, J. Chem. Phys. 31, 459 (1959).

[2]A. Rahman, Phys. Rev. 136, A405 (1964).

[3]B. J. Berne and G. D. Harp, Advan. Chem. Phys. 17, 63 (1970).

[4]L. Verlet, Phys. Rev. 159, 98 (1967).

[5]L. Verlet, Phys. Rev. 165, 209 (1968).

[6]D. Levesque and L. Verlet, Phys. Rev. A 2, 2514 (1970).

[7]G. D. Harp and B. J. Berne, Phys. Rev. A 2, 975 (1970).

[8]A. Rahman and F. H. Stillinger, J. Chem. Phys. 55, 3336 (1971).

[9]J. R. Sweet and W. A. Steele, J. Chem. Phys. 47, 3022 (1967).

[10]O. Schnepp and A. Ron, Discussions Faraday Soc. 48, 26 (1969).

[11]J. C. Laufer, Ph.D. thesis (Preston University, 1969) (unpublished).

[12]B. Quentrec and C. Brot, J. Chem. Phys. 54, 3655 (1971).

[13]A. Van Itterbeek and O. Verbeke, Physica 26, 931 (1960).

[14]L. Verlet and J. J. Weis, Phys. Rev. A 5, 939 (1972).

[15]J. J. Weis and D. Schiff (private communication).

[16]S. Sung and D. Chandler, J. Chem. Phys. 56, 4989 (1972).

[17]D. G. Henshaw, D. G. Hurst, and N. K. Pope, Phys. Rev. 92, 1229 (1953).

[18]H. W. Furumoto and C. H. Shaw, Phys. Fluids 7, 1026 (1964). Tabulated by P. W. Schmidt and C. W. Tompson in *Simple Dense Fluids*, edited by H. L. Frisch and Z. W. Salsburg (Academic, New York, 1968).

[19]R. G. Gordon, Advan. Mag. Res. 3, 1 (1968).

[20]R. G. Gordon, J. Chem. Phys. 42, 3658 (1965).

[21]M. F. Crawford, H. L. Welsh, and J. H. Harrold, Can. J. Phys. 30, 81 (1952).

[22]A. S. DeReggi, P. C. Canepa, and T. A. Scott, J. Mag. Res. 1, 144 (1969).

[23]V. F. Sears, Can. J. Phys. 44, 1279 (1966).

[24]R. Zwanzig, in *Lectures in Theoretical Physics*, edited by W. E. Brittin, W. B. Downs, and J. Downs (Interscience, New York, 1961), Vol. 3, p. 135.

[25]H. Mori, Progr. Theoret. Phys. (Kyoto) 34, 399 (1965).

[26]R. Zwanzig and M. Bixon, Phys. Rev. A 2, 2906 (1970).

[27]D. Levesque and L. Verlet, Phys. Rev. A (to be published).

[28]P. Debye, *Polar Molecules* (Dover, New York, 1928).

[29]W. Kauzmann, Rev. Mod. Phys. 14, 12 (1942).

[30]E. N. Ivanov, Zh. Eksperim. i Teor. Fiz. 45, 1509 (1963) [Sov. Phys. JETP 18, 1041 (1964)].

[31]C. Brot, J. Phys. 28, 789 (1967).

[32]B. Lassier and C. Brot, Chem. Phys. Letters 1, 581

(1968).
[33]R. G. Gordon, J. Chem. Phys. 44, 1830 (1966).
[34]R. E. McClung, J. Chem. Phys. 51, 3842 (1969).
[35]G. D. Harp and B. J. Berne, J. Chem. Phys. 49, 1249 (1968).
[36]B. J. Berne, J. Chem. Phys. 56, 2164 (1971).

PHYSICAL REVIEW A VOLUME 7, NUMBER 3 MARCH 1973

Multiple Exchange in the Quantum Crystals*

A. K. McMahan† and R. A. Guyer
Department of Physics and Astronomy, University of Massachusetts, Amherst, Massachusetts 01002
(Received 11 October 1972)

We develop the generalization of the Heisenberg near-neighbor-exchange Hamiltonian necessary to incorporate the effects of multiple-exchange processes. Many-body expressions for the multiple-exchange constants (pair exchange, triple exchange, and quadruple exchange) are derived. The physics that enters these exchange constants is discussed. For the most important of the pair and triple cases, these expressions are carefully evaluated using a Monte Carlo integration scheme. We show that the exchange Hamiltonian for solid ^{3}He is rapidly convergent, and that the near-neighbor pair, next-near-neighbor pair, and triple-exchange processes (involving two near neighbors and a next-near neighbor) are likely to be the only important exchange processes to the low-temperature thermodynamics of bcc ^{3}He. The magnitude of the triple-exchange process is such that the "effective" next-near-neighbor pair-exchange interaction in bcc ^{3}He is ferromagnetic. This result provides qualitative and quantitative support to the explanation of the data of Kirk and Adams made by Zane.

I. INTRODUCTION

A quantum crystal is a crystal in which the zero-point displacement of a particle, $\sqrt{\langle u^2\rangle}$, is a substantial fraction of the near-neighbor distance Δ. Quite surprisingly, there are many macroscopic properties of the best-known quantum crystals (solid ^{3}He and solid ^{4}He) which appear relatively unaffected by this large zero-point motion. Simple thermostatic measurements, e.g., specific heat, thermal conductivity, etc., yield evidence for properties that are much like those of similar nonquantum crystals.[1] The truly unique experimental properties of the quantum crystals, however, are a consequence of the large zero-point motion, as manifested in the tunneling motions of the constituent particles. The wide variety of motionally narrowed nuclear magnetic resonance (NMR) phenomena in solid ^{3}He provide ample evidence for the presence of these tunneling motions.[2] The dominant motion that leads to this narrowing is the cooperative tunneling of a pair of near-neighbor ^{3}He atoms past one another, the exchange process. In crystals with vacancies, the tunneling of ^{3}He particles into vacant lattice sites leads to vacancy waves.[3] In crystals containing isotopic impurities the cooperative tunneling of an impurity atom and a neighboring host atom leads to "impuritons"[4] or "mass-fluctuation waves" (for dilute ^{3}He in ^{4}He).[2,5]

A discussion of the excitations that are a consequence of tunneling or a discussion of systems containing these excitations proceeds on two levels. *First* a qualitative description of the physics can proceed from an assumed form for a model Hamiltonian or an assumed form for the dispersion relation. The work of Andreev and Lifshitz,[4] on "defectons" and "impuritons", Guyer and Zane[5] on "mass-fluctuation waves" and Guyer, Richardson, and Zane[2] in explanation of NMR phenomena are in terms of systems of excitations whose quantitative parameters are assumed known. For example, the behavior of solid ^{3}He at low temperatures is taken to be that of a near-neighbor Heisenberg antiferromagnet with the value of J being determined by experiment. *Second*, the model Hamiltonians employed in qualitative descriptions must be formally justified and a rigorous determination of the parameters that enter them must be implemented. These parameters depend strongly on the wave function of the system so that their determination constitutes an important test of the solution of the wave-function problem.

The near-neighbor pair-exchange Heisenberg Hamiltonian has in the past proved quite adequate in theoretical analyses of the thermodynamic[6,7] and NMR properties[2,8] of solid ^{3}He. An extensive literature[9–17] exists which reports calculations of the corresponding exchange parameter J, and adequate agreement with experiment has generally been obtained. We briefly review some of the recent progress reported in this literature later in this section. Recently, however, the excess pressure of solid ^{3}He in strong external magnetic fields has been measured by Kirk and Adams,[18] and found to be in disagreement with the predictions of the usual *near-neighbor pair-exchange* Heisen-